Intermittency Route to Rheochaos in Wormlike Micelles with Flow-Concentration Coupling

Rajesh Ganapathy and A. K. Sood

Department of Physics, Indian Institute of Science, Bangalore 560012, India

(Received 7 November 2005; published 14 March 2006)

We show experimentally that the route to chaos is via intermittency in a shear-thinning wormlike micellar system of cetyltrimethylammonium tosylate, where the strength of flow-concentration coupling is tuned by the addition of salt sodium chloride. A Poincaré first return map of the time series and the probability distribution of laminar lengths between burst events shows that our data is consistent with type-II intermittency. The coupling of flow to concentration fluctuations is evidenced by the ''butterfly'' intensity pattern in small angle light scattering (SALS) measurements performed simultaneously with the rheological measurements. The scattered depolarized intensity in SALS, sensitive to orientational order fluctuations, shows the same time dependence (like intermittency) as that of shear stress.

DOI: 10.1103/PhysRevLett.96.108301 PACS numbers: 82.70.Uv, 82.70.Gg, 83.85.Ei, 83.85.St

Rheochaos—irregular time variation in the stress/shear rate at a constant shear rate/stress arising from nonlinearities in the viscoelastic constitutive equations—was first observed [1] in shear-thinning wormlike micelle solutions. This has led to many theoretical [2–6] and experimental studies of this striking effect in a wide variety of other systems including shear-thickening wormlike micellar solutions [7], lamellar, onion, and sponge phases of surfactants [8] and dense colloidal suspensions [9]. NMR velocimetry and rheo-optical experiments [10] suggest that rheochaos is closely linked to the phenomenon of shear banding. Above a critical shear rate $\dot{\gamma}_c$, microscopic models for wormlike micelles [11] predict a decrease in stress (σ) with further increase in the shear rate ($\dot{\gamma}$), rendering homogenous flow unstable. This gives rise to the coexistence of high and low shear rate bands at a common stress and shows up as a stress plateau in the flow curve. It has been shown in [10] that the interface between the shear rate bands is not stable as predicted [11], but shows complex spatiotemporal dynamics and this is accompanied by stress/shear rate fluctuations. In this Letter we answer a crucial question that has remained unaddressed in experiments so far: *what is the route to rheochaos?* Our primary observations are summarized in Figs. 2 and 3, where we show that the route to rheochaos is via intermittency for a system of wormlike micelles with strong coupling of flow to concentration fluctuations. We also establish, using SALS measurements, the vital role played by the nematic alignment of the wormlike micelles (see Fig. 4) in rheochaos.

Some background material will be useful here. There are three routes to chaos: the period-doubling route, the quasiperiodic route, and the intermittency route. The intermittency route is characterized by bursts of chaos disrupting nearly periodic (laminar region) oscillations. Pomeau and Manneville [12] have established that within the intermittency route there are further three types. Type-I appears with a inverse tangent bifurcation, Type-II with a Hopf bifurcation, and Type-III is associated with a period-doubling bifurcation. Experimentally, all three types of intermittency have been observed in a variety of hydrodynamical and electrical systems [13], although there are fewer examples of Type-II intermittency which sets in via quasiperiodicity. Our experiments, we show below, are consistent with Type-II intermittency route to chaos.

In a recent theoretical study, Fielding and Olmsted [14] have taken into account the effect of concentration coupling in shear banding wormlike micellar systems that are far from a zero-shear isotropic-nematic (I-N) transition. Their model predicts a positive value for the slope of the plateau in the banded region of the flow curve, and the slope increases with the strength of the coupling between flow and concentration fluctuations. In a recent experimental work, Bandyopadhyay and Sood [15] have shown that the slope α of the stress plateau, which we find is a power law ($\sigma \sim \dot{\gamma}^{\alpha}$), for wormlike micellar solutions of surfactant cetyltrimethylammonium tosylate (CTAT) can be tuned by adding salt (NaCl). These results motivated us to study the consequences of flow-concentration coupling on the stress relaxation dynamics in this class of systems.

The phase behavior of CTAT has been well characterized [16]. Above the Krafft temperature of 23 °C and at concentrations ($0.04\ \text{wt}\% < c < 0.4\ \text{wt}\%$) cylindrical micelles are formed which, at $c > c_* = 0.4\ \text{wt}\%$, entangle to form viscoelastic gels. The CTAT/water and CTAT/NaCl/water samples were prepared by dissolving known amounts of CTAT (Sigma Aldrich) in water and brine, respectively, and this study mainly focuses on the later. The samples were filtered through 200 nm pore size filters to remove dust impurities and left to equilibrate for two days. The experiments were carried out on a MCR 300 stress-controlled rheometer (Anton PAAR, Germany) with a small angle light scattering attachment (SALS) at a temperature of 26.5 °C. The rheometer was used in the feedback mode for strain-controlled experiments. All experiments were carried out in a cylindrical Couette geometry with top and bottom windows made of quartz glass (inner cylinder diameter 32 mm, height 16.5 mm, and gap 2 mm). A vertically polarized (V) laser beam ($\lambda = 658$ nm and spot size 1 mm) enters the gap between the cylinders

(the beam is close to the inner rotating cylinder and cannot be translated across the gap) along the vorticity ($\nabla \times \mathbf{v}$) direction, where $\mathbf{v}$ is the velocity field. An analyzer below the Couette geometry allows us to select either the vertically (VV) or the horizontally polarized (VH) scattered light from the sample. A condenser beneath the analyzer collects the scattered light dominantly from a plane 6 mm above the bottom plate and forms the image on a screen in the ($\mathbf{v}$, $\nabla\mathbf{v}$) plane. The imaging was done using a 8-bit color CCD camera (Lumenera 075C, 640×480 pixels, maximum frame rate -60 fps) at a frame rate of 1 frame/750 ms. About 3000 images were grabbed for each polarization while stress relaxation measurements were simultaneously going on. The intensity at various wave vectors from the noise filtered image was analyzed.

We now turn to our results. Figure 1(a) (filled circles) shows the flow curve for CTAT 2 wt% in a controlled-stress experiment. The flow curve shows a near plateau for $\dot{\gamma} > 0.1\ \mathrm{s}^{-1}$. The observed weak departure (slope $\alpha = 0.07$ in the log-log plot) from a true plateau is very likely due to the small inhomogeneity of the stress field arising from curvature effects in the cylindrical Couette geometry [14,17]. Figure 1(a) also shows the flow curve for CTAT 2 wt% + 100 mM NaCl (hollow circles). The stress shows a much stronger shear rate dependence [$\alpha = 0.32$ for CTAT 2 wt% + 100 mM NaCl and $\alpha = 0.24$ for CTAT 2 wt% + 50 mM NaCl. See Fig. 1(a) inset] above $\dot{\gamma} > 1\ \mathrm{s}^{-1}$, which cannot be due to geometry effects alone [14]. We attribute this slope to a concentration difference between the shear rate bands [14,18]. Our system is in the semidilute region and is far from a zero-shear *I*-*N* transition ≈ 27 wt% for pure CTAT [16] and >30 wt% for CTAT + 50 mM NaCl. Hence, a large slope α is not due to *I*-*N* coexistence [19]. A concentration difference between the shear rate bands can arise from a Helfand-Fredrickson mechanism [20]. Here, the high shear rate band is predicted to be lower in concentration due to micelles diffusing against their own concentration gradients leading to flow-enhanced concentration fluctuations. If so, our SALS experiments should show a "butterfly" light scattering pattern with the wings of the butterfly stretched along the flow direction [21]. Figure 1(b) shows the SALS pattern in VV geometry for CTAT 2 wt% and CTAT 2 wt% + 100 mM NaCl. The butterfly pattern is absent for the pure CTAT 2 wt% [Fig. 1(b)(i)] and is present for CTAT 2 wt% + 100 mM NaCl [Fig. 1(b)(ii)], and (iii) and (iv) in Fig. 1(b) show corresponding patterns in VH geometry. We have carried out experiments at six different salt concentrations $10\ \mathrm{mM} < c_{\mathrm{NaCl}} < 1\ \mathrm{M}$, which yield plateau slopes ranging from $0.07 < \alpha < 0.4$. We find that a minimum slope of 0.12, corresponding to a salt concentration of 25 mM NaCl, is essential to see a butterfly pattern indicating the onset of flow concentration coupling at this α value.

Figs. 2(a)–2(c) show the stress relaxation dynamics for three shear rates fixed in the plateau region for the system CTAT 2 wt% + 100 mM NaCl. Figure 2(a) shows the stress relaxation dynamics at $\dot{\gamma} = 23\ \mathrm{s}^{-1}$. The signal looks periodic, but a closer inspection reveals finer features that do not repeat exactly. Figure 2(d) shows the power spectrum of this signal. Apart from the two primary frequencies centered around $\omega_1 = 0.049$ and $\omega_2 = 0.061$ Hz and their higher harmonics, there are other frequency components centered at linear combinations of ω_1 and ω_2 like $\omega_2 - \omega_1$ and $\omega_1 + \omega_2$. These extra features are the hallmark of a two-frequency quasiperiodic signal [22,23]. In Fig. 2(b), there are bursts of chaos breaking in between the quasiperiodic signal for $\dot{\gamma} = 25\ \mathrm{s}^{-1}$. The power spectrum of the quasiperiodic laminar region once again shows two frequencies centered around $\omega_1 = 0.057$ and $\omega_2 = 0.063$ Hz, implying a decrease in the time period with increasing shear rate. The stress relaxation dynamics at $\dot{\gamma} = 27.5\ \mathrm{s}^{-1}$ [Fig. 2(c)] was completely chaotic (characterized by a positive Lyapunov exponent ≈ 0.14 and an

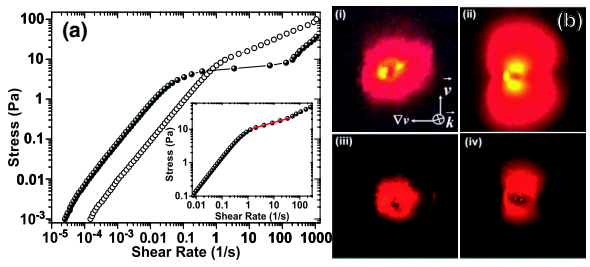

FIG. 1 (color online). (a) Flow curves for CTAT 2 wt% (solid circles) and CTAT 2 wt% + 100 mM NaCl (hollow circles). Inset: Flow curve for CTAT 2 wt% + 50 mM NaCl (red line: linear fit). (b) SALS profiles (i) and (iii) CTAT 2 wt% for VV and VH polarizations. (ii) and (iv) CTAT 2 wt% + 100 mM NaCl for VV and VH polarizations.

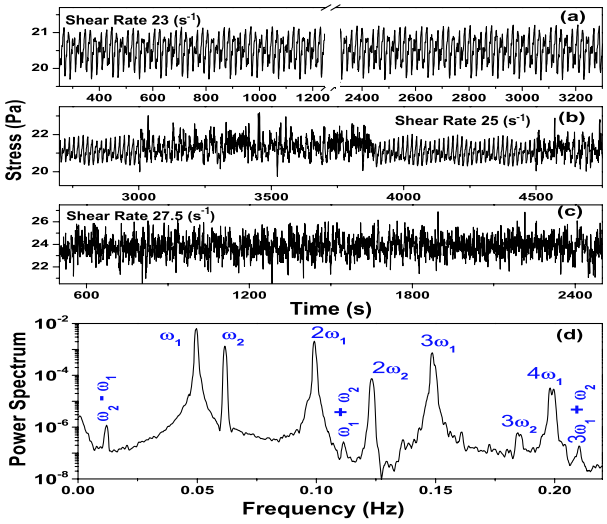

FIG. 2 (color online). Stress relaxation dynamics for CTAT 2 wt% + 100 mM NaCl for different shear rates. (a) $\dot{\gamma} = 23\ \mathrm{s}^{-1}$, (b) $\dot{\gamma} = 25\ \mathrm{s}^{-1}$, (c) $\dot{\gamma} = 27.5\ \mathrm{s}^{-1}$, and (d) Fourier power spectrum of (a).

exponential Fourier power spectrum [24]). Although the exact shear rate values at which the sample displayed the above features was found to differ to some extent from run to run; the main features, namely, quasiperiodic oscillations and intermittent bursts were found in all the runs. All systems with $\alpha \geq 0.12$, implying moderate to strong flow-concentration coupling, showed quasiperiodicity and intermittency. Figure 3(a) shows the partial time series at $\dot{\gamma} = 22\ s^{-1}$ obtained during a different run. Judging by the nature of the signal during the laminar phase, Type-III intermittency can be ruled out, since, for this type of intermittency there is a subharmonic mode with increasing amplitude. We follow the method described in [25] and reconstruct a Poincaré plot by taking the successive minima of the stress in the laminar region after a chaotic burst. In Fig. 3(c), we plot the value of the stress at the Nth minimum against its value at the $(N-1)$th minimum. This plot exhibits a spiraling behavior characteristic of Type-II intermittency. The spiraling behavior is time inverted and we call this time inverted Type-II intermittency after [26] who found similar behavior in a semiconductor laser with external feedback. The above behavior implies that the system oscillates back to the laminar phase after a disturbance that caused a burst event. A standard test for Type-II intermittency is the probability distribution of laminar lengths L between burst events that scales as $P(L) \sim L^{-2}$ for small times and shows an exponential tail at larger times [27]. This test could not be carried out for the above mentioned time series due to an insufficient number of burst events. In Fig. 3(b) we show the time series obtained for CTAT 2 wt % + 50 mM NaCl ($\alpha = 0.24$) at $\dot{\gamma} = 19\ s^{-1}$ which shows about 50 bursts in a 2 hr run. The probability distribution of laminar lengths clearly shows the exponential tail [Fig. 3(d)] expected at large times. This test rules out Type-I intermittency, for which $P(L)$ increases at longer times [27], and confirms the Type-II intermittency route to chaos in the present study.

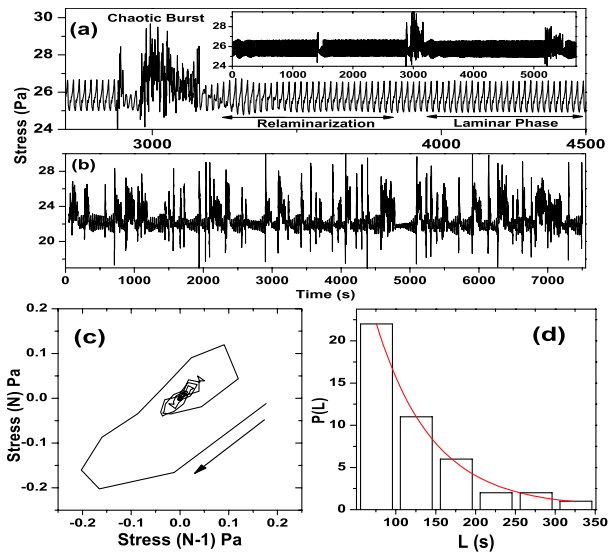

FIG. 3 (color online). (a) Partial stress time series for CTAT 2 wt % + 100 mM NaCl at $\dot{\gamma} = 22\ s^{-1}$ for a different run. Inset: Full time series. (b) Complete stress time series for CTAT 2 wt % + 50 mM NaCl at $\dot{\gamma} = 19\ s^{-1}$. (c) First return Poincaré plot for (a). The arrow shows the spiraling direction. (d) Probability distribution of laminar lengths between bursts for (b). The line is an exponential fit.

Recent theoretical attempts to explain rheochaos treat our systems as nematogenic fluids, and consider the spatiotemporal evolution of the shear stress associated with the nematic order parameter [2,3,6]. These models, while ignoring the complexities of breakage, flexibility, and branching, capture the essential flow-induced orientability of wormlike micelles. Light scattering measurements in the VH geometry are sensitive to orientational fluctuations, while VV geometry is influenced by concentration and orientational order fluctuations. We describe below the results of these measurements.

SALS measurements were done with VV polarization for half the duration and VH polarization for the remaining half of the stress relaxation run. The appearance of an *anisotropic* VH scattering pattern in our SALS measurements [Fig. 1(b)(iv)] at the onset of shear-thinning implies that our systems are nematic. The time series for VV and VH intensities at a fixed wave vector, $q = 0.75\ \mu m^{-1}$, are shown in Figs. 4(a)–4(c). Figures 4(a) and 4(b) show the time series of VV and VH intensities obtained during the stress relaxation measurement shown in Fig. 2(a). Qualitatively, the VH intensity follows oscillations in the stress whereas VV does not. A power spectrum of the VH time series shows that the two primary frequency components (ω_1, ω_2) coincide with those obtained from the stress time series. The frequency components at $\omega_2 - \omega_1$, $\omega_1 + \omega_2$ and $3\omega_1 + \omega_2$ shown in Fig. 2(d) for the stress are absent. This may be due to the averaging procedure we have used to remove CCD noise. Figure 4(c) shows the VH time series for $\dot{\gamma} = 25\ s^{-1}$. This time series captures the quasiperiodicity as well the chaotic burst seen in the corresponding stress relaxation measurement [Fig. 2(b)]. At higher shear rates the VH time series was chaotic. We also observe that the entire VH profile shows periodic breathing patterns for $\dot{\gamma} = 23\ s^{-1}$ and $\dot{\gamma} = 25\ s^{-1}$. This has been quantified by measuring the anisotropy (ϵ_s) and the orientation angle (χ_s) obtained from the second moment tensor of $S_{VH}(q, t)$ [28] given by, $\epsilon_s = [(\langle XX\rangle - \langle YY\rangle)^2 + 4\langle XY\rangle^2]^{1/2}$ and $\tan(2\chi_s) = \frac{2\langle XX\rangle}{\langle XX\rangle - \langle YY\rangle}$, where $\langle XY\rangle = \int d\mathbf{q} q_X q_Y S_{VH}(q, t)$, $\langle XX\rangle = \int d\mathbf{q} q_X q_X S_{VH}(q, t)$ and $\langle YY\rangle = \int d\mathbf{q} q_Y q_Y S_{VH}(q, t)$. Figures 4(d) and 4(e) show the time series of the anisotropy and orientation angle at $\dot{\gamma} = 25\ s^{-1}$. The anisotropy and the orientation angle of the major axis of $S_{VH}(q, t)$, which is a measure of the instantaneous orientation of the nematics, seems to follow the stress oscillations [Fig. 2(b)]. The orientation angle shows regular oscillations from $\approx 20°$ to $\approx 80°$ when the system is in the laminar or quasiperiodic region and shows no periodicity when the system shows a chaotic burst.

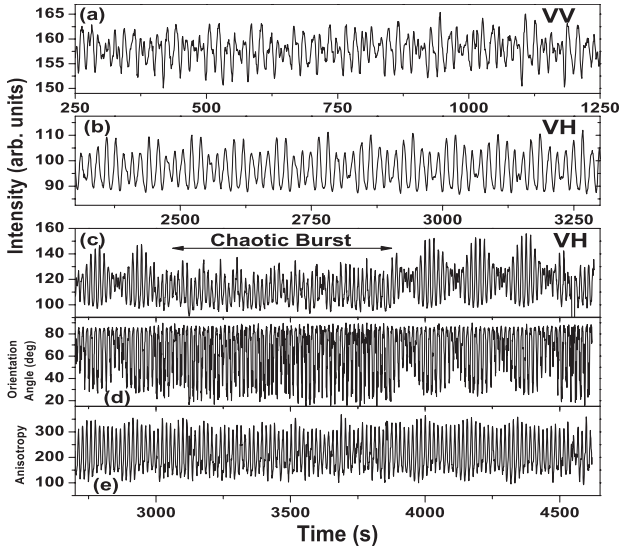

FIG. 4. The VV intensity time series (a) and the VH intensity time series (b) for CTAT 2 wt% + 100 mM NaCl at a $\dot{\gamma} = 23\ s^{-1}$. Experiment was done with VV polarization to the left of the break shown in the stress time series [Fig. 2(a)] and with VH polarization to the right. (c) The VH intensity time series at a $\dot{\gamma} = 25\ s^{-1}$ [see Fig. 2(b)]. (d) and (e) show the anisotropy and the orientation angle of $S_{VH}(q, t)$ for (c).

To summarize, we have shown for the first time, intermittency in stress relaxation dynamics for the systems that show coupling between flow and concentration. We have also shown that the VH intensity at a fixed wave vector, anisotropy, and the orientation angle shows dynamics similar to the dynamics seen in stress oscillations. In all our experiments, the butterfly pattern is always accompanied by intermittency in stress dynamics. We believe it is essential to have flow-concentration coupling to observe the rich dynamics we have seen since this could provide a mechanism by which mechanical shear banding instabilities could crossover to shear induced demixing instabilities [5,14]. To the best of our knowledge, there are no theoretical models that predict temporal intermittency in the stress for wormlike micelles that show shear banding. Interestingly, in the rheochaos model by Fielding and Olmsted [5], spatiotemporal intermittent behavior is seen for moderate to strong coupling strength between the flow and the micellar length. The spatiotemporal intermittency route to chaos has also been predicted by [6]. A complete theoretical understanding for temporal intermittent behavior in systems that show flow-concentration coupling is lacking at the moment. Our experiments further reinforce the case that rheochaos, far from being mere irregularity in the flow of a complex fluid, lies squarely in the domain of chaotic nonlinear dynamical systems. We hope that our results will motivate further experiments and theoretical modeling.

We thank Professor Sriram Ramaswamy for fruitful discussions.

[1] R. Bandyopadhyay *et al.*, Phys. Rev. Lett. **84**, 2022 (2000).
[2] M. Grosso *et al.*, Phys. Rev. Lett. **86**, 3184 (2001).
[3] G. Rienacker *et al.*, Phys. Rev. E **66**, 040702 (2002).
[4] D. A. Head *et al.*, Phys. Rev. E **64**, 061509 (2001); M. E. Cates *et al.*, Phys. Rev. E **66**, 025202(R) (2002); A. Aradian and M. E. Cates, Europhys. Lett. **70**, 397 (2005).
[5] S. M. Fielding and P. D. Olmsted, Phys. Rev. Lett. **92**, 084502 (2004).
[6] B. Chakrabarti *et al.*, Phys. Rev. Lett. **92**, 055501 (2004); M. Das *et al.*, Phys. Rev. E **71**, 021707 (2005).
[7] R. Bandyopadhyay and A. K. Sood, Europhys. Lett. **56**, 447 (2001); P. Fisher, Rheol. Acta **39**, 234 (2000).
[8] A. S. Wunenburger *et al.*, Phys. Rev. Lett. **86**, 1374 (2001); J.-B. Salmon *et al.*, Phys. Rev. E **66**, 031505 (2002); L. Courbin *et al.*, Phys. Rev. Lett. **92**, 018305 (2004).
[9] D. Lootens *et al.*, Phys. Rev. Lett. **90**, 178301 (2003).
[10] M. R. López-Gonzaleź *et al.*, Phys. Rev. Lett. **93**, 268302 (2004); W. M. Holmes *et al.*, Europhys. Lett. **64**, 274 (2003); J.-B. Salmon *et al.*, Phys. Rev. E **68**, 051504 (2003).
[11] N. A. Spenley *et al.*, Phys. Rev. Lett. **71**, 939 (1993).
[12] Y. Pomeau and P. Manneville, Commun. Math. Phys. **74**, 189 (1980).
[13] C. Jeffries and J. Perez, Phys. Rev. A **26**, 2117 (1982); M. Dubois *et al.*, Phys. Rev. Lett. **51**, 1446 (1983); J.-Y. Huang and J.-J. Kim, Phys. Rev. A **36**, 1495 (1987).
[14] S. M. Fielding and P. D. Olmsted, Eur. Phys. J. E **11**, 65 (2003).
[15] R. Bandyopadhyay and A. K. Sood, Langmuir **19**, 3121 (2003).
[16] J. F. A. Soltero and J. E. Puig, Langmuir **11**, 3337 (1995).
[17] The increase in stress due to geometry curvature calculated from [14] is $\delta\sigma \approx 1.3$ Pa for CTAT 2 wt% which is in good agreement with the change we observe in experiment ≈ 1.6 Pa.
[18] V. Schmitt *et al.*, Phys. Rev. E **52**, 4009 (1995).
[19] J. F. Berret *et al.*, Europhys. Lett. **25**, 521 (1994).
[20] E. Helfand and G. H. Fredrickson, Phys. Rev. Lett. **62**, 2468 (1989); S. T. Milner, Phys. Rev. Lett. **66**, 1477 (1991); M. Doi and A. Onuki, J. Phys. II (France) **2**, 1631 (1992).
[21] I. A. Kadoma and J. W. van Egmond, Phys. Rev. Lett. **76**, 4432 (1996); Phys. Rev. Lett. **80**, 5679 (1998).
[22] E. Ott, *Chaos in Dynamical Systems* (Cambridge University Press, Cambridge, England, 1993), 2nd ed.
[23] The linewidths in the power spectrum decrease with increase in length of the time series, showing that they are transform limited.
[24] H. S. Greenside *et al.*, Physica D (Amsterdam) **5**, 322 (1982).
[25] P. Bergé *et al.*, *Order Within Chaos* (Hermann, Paris, 1984).
[26] J. Sacher *et al.*, Phys. Rev. Lett. **63**, 2224 (1989).
[27] H. G. Schuster, *Deterministic Chaos* (VCH, Weinheim, 1988).
[28] I. A. Kadoma and J. W. van Egmond, Langmuir **13**, 4551 (1997).